An agent-based model of molecular aggregation at the cell membrane

Juliette Griffié[ID]*, **Ruby Peters, Dylan M. Owen***

Department of Physics and Randall Centre for Cell and Molecular Biophysics, King's College London, London, England, United Kingdom

* juliette.griffie@kcl.ac.uk (JG); dylan.owen@kcl.ac.uk (DO)

Abstract

Molecular clustering at the plasma membrane has long been identified as a key process and is associated with regulating signalling pathways across cell types. Recent advances in microscopy, in particular the rise of super-resolution, have allowed the experimental observation of nanoscale molecular clusters in the plasma membrane. However, modelling approaches capable of recapitulating these observations are in their infancy, partly because of the extremely complex array of biophysical factors which influence molecular distributions and dynamics in the plasma membrane. We propose here a highly abstracted approach: an agent-based model dedicated to the study of molecular aggregation at the plasma membrane. We show that when molecules are modelled as though they can act (diffuse) in a manner which is influenced by their molecular neighbourhood, many of the distributions observed in cells can be recapitulated, even though such sensing and response is not possible for real membrane molecules. As such, agent-based offers a unique platform which may lead to a new understanding of how molecular clustering in extremely complex molecular environments can be abstracted, simulated and interpreted using simple rules.

Introduction

The plasma membrane (PM) has long been identified as a key component of cellular machinery. Its function is not limited to separating intra-cellular organelles from the extracellular environment; it is also recognized broadly as the principal instigator and coordinator of inter-cellular interactions[1, 2]. The PM has been shown, for instance, to be involved in signalling pathway activation and inter-cell communication[3–5]. Processes such as neuronal transmission[6, 7], the triggering of an immune response[8–10], Ras regulated pathways associated with mammalian cell survival and proliferation[11–13] and others, rely heavily on the molecular organisation at the PM.

In practice, molecular clustering has been highlighted as important in regulating signal transduction at the PM. Its study has benefited considerably from the rise of fluorescence microscopy and more recently super resolution methods[14–16], enabling, for the first time, the visualisation of molecular aggregation at the nanoscale. In fact, relatively small changes in the clustering configuration of signalling proteins, i.e. variations in their spatio-temporal

organisation at the PM, are thought to be necessary and/or sufficient for the initiation of downstream signalling, a process commonly referred to as digitization[17–19]. Interestingly, identifying the biological processes driving molecular aggregation at the plasma membrane remains an open question. Their often competing roles are also poorly understood and can't easily explain, or be used to model, observed molecular distributions.

Considering the current interest of the community in molecular aggregation at the PM, its understanding at a more theoretical level remains relatively understudied and simplified models are generally lacking or focusing on a specific activation pathway in a given cell type[20]. Agent-based models have been used across a wide variety of fields successfully to understanding collective behaviour, including in sociology[21], crowd management[22] and economics [23–25]. In this work, we develop an agent-based model dedicated to the study of molecular aggregation in the PM. The strength of such models with high levels of abstraction, such as the agent-based approach, is that they propose general rules otherwise inaccessible in complex systems. In our case, this translates to results being independent of cell type or signalling pathway. As such, the model presented here uniquely provides a platform in which one can study how to generate and modify molecular aggregation within a pre-set framework.

Our hypothesis is that all competing factors affecting a given molecular population distribution at the cellular membrane can be summarised as a single "desire for clustering" assigned to each agent (i.e. molecule). We demonstrate that this overall "desire for clustering" translated in an agent-based model, is sufficient to recapitulate clustering behaviours observed in cellular membranes. While in reality, molecules are not able to sense their neighbours at distances of tens or hundreds of nanometres, we show that they behave *as if* they can. We show that this apparent behaviour can be exploited to construct simplified models which recapitulate clustering profiles without the new to incorporate a full biophysical model. Interestingly, we also demonstrate that a modification of the environment, for instance a filamentous actin enriched environment, leads to distinct modifications of the clustering patterns as observed in cells.

Model

The theoretical framework

Any agent-based model relies on three levels of abstraction. It consists of an observer (or user) defining an environment (the PM in our case) in which agents (here, the diffusing molecules) evolve following pre-set rules. The model thus allows studying the fate of these agents over time (the third level of abstraction).

In practice, for simulations we consider 2000 agent-molecules diffusing freely (i.e. following Brownian motion) in a 2D 3 x 3 μm^2 region of interest (ROI: the PM). Initially all proteins are randomly distributed forming a completely spatially random (CSR) distribution. The boundaries of the ROI are toroidally wrapped to ensure a constant number of molecules. The mobility characteristics of each molecule are updated every 10 ms. The simulations are run for 5 minutes (i.e. a total of 30,000 updated frames) as most cellular processes occur in this range of timescales. In all cases studied, n = 30 simulations were generated.

Although a multitude of cellular processes have been shown to promote molecular clustering in cellular membranes, our initial hypothesis is that they can be summarised by a unique parameter: the "desire for clustering" given to each agent. This "desire" parameter results from a combination of competing cellular processes ranging from self-affinity, membrane lipid domains[26–32], the size exclusion model[33] and the picket-fence model[34] to name a few. It is this "desire for clustering" that constitutes the pre-set rules applied to each agent.

Imposing pre-set rules on the agents: The "desire for clustering"

The method by which we generate a "desire for clustering" for each agent is by imposing a rate of Brownian motion, which is dependent on the immediate density of that agent's local molecular environment. All agents possess a theoretical "target value" for clustering (defined as a certain number of neighbours within a 100 nm radius) and the closer its local density is to the targeted value, the slower the agent. Hence, whilst maintaining the assumption of molecules diffusing freely following Brownian motion in the PM, the diffusion coefficient (DC) of each molecule is fixed according to the local level of clustering.

For each frame and for each ith localisation, the local density is estimated based on the "L_R" value, i.e. the linearised localised Ripley's K function:

$$L_R = \sqrt{\frac{A}{n \times \pi} \times \sum \delta_{i,j}}$$

Where A is the area of the ROI, n is the total number of molecules in the ROI, for $i \neq j$, $\delta_{i,j} = 1$ if the molecule j is contained in a circle of radius R centred on molecule i and $\delta_{i,j} = 0$ otherwise. Here, we define $R = 100$ nm, as molecular clusters in cellular membranes have been shown to be typically below the diffraction limit of light (< 200nm)[12, 35–37]. L_R is a mathematically well-defined quantity, considered as an accurate measure of local density and routinely used for spatial point pattern (SPP) cluster analysis [12, 38–40]. For a CSR distribution, the average L_R value equals R (in our case $L_{100} \sim 100$, translating into 7 molecules encircled within 100 nm of each molecule). This is the starting point of the simulations (Fig 1a).

The target value for the clustering of all agents is simply defined as a specific value of L_{100}. For each agent-molecule i, the measured value of $L_{100,i}$ can therefore be compared to that target, from which the step displacement (D) per second is updated independently for each agent-molecule in every frame. Each molecule is thus attributed an independent D as a result of the level of clustering (L_{100}), ranging from a pre-defined maximum (D_{max}) to a minimum value when the agent reaches the targeted L_{100}. Although the resulting diffusion is an approximation for Brownian motion, the difference in order of magnitude between step displacement (given the update/frame rate) and the length scale at which we study cluster formation, ensures this approximation is robust. Multiple functions can be chosen to map the dependence of D on L_{100}. For the Standard Condition, we focus on a linearly converging profile in which a molecule i that has been attributed $L_{100,i} >= L_{100,target}$ is set as fully immobile (i.e. $D_{min} = 0$) as illustrated in Fig 1b. Our overall model is summarized in Fig 1c.

After running the model, a number of outputs are generated. Principal among these are the average values of L_{100} per frame of the simulation, serving as a measure of the overall level of clustering within the ROI (referred to as $< \widehat{L}_{100} >$). From the agent-molecule coordinates we can also extract more detailed clustering descriptors using a Bayesian based approach with topographic prominence thresholding[41–44]. These include the number of clusters, percentage of molecules in clusters, cluster radius and the number of molecules per cluster.

Results

The agent-based model leads to molecular aggregation

We first determined whether or not the "desire for clustering" is sufficient to induce measured clustering. For our Standard Condition displacement profile (Fig 1b), we fix Dmax at 3.5 nm. ms^{-1} which translates to a DC of ~0.1 $\mu m^2.s^{-1}$, i.e. within the range of expected values for transmembrane proteins (typically varying from 0.01 $\mu m^2.s^{-1}$ to 1 $\mu m^2.s^{-1}$)[45–47] and Dmin = 0 (i.e. fully immobile). We varied the targeted L_{100} from 7 encircled molecules ($L_{100} \sim 100$, the CSR
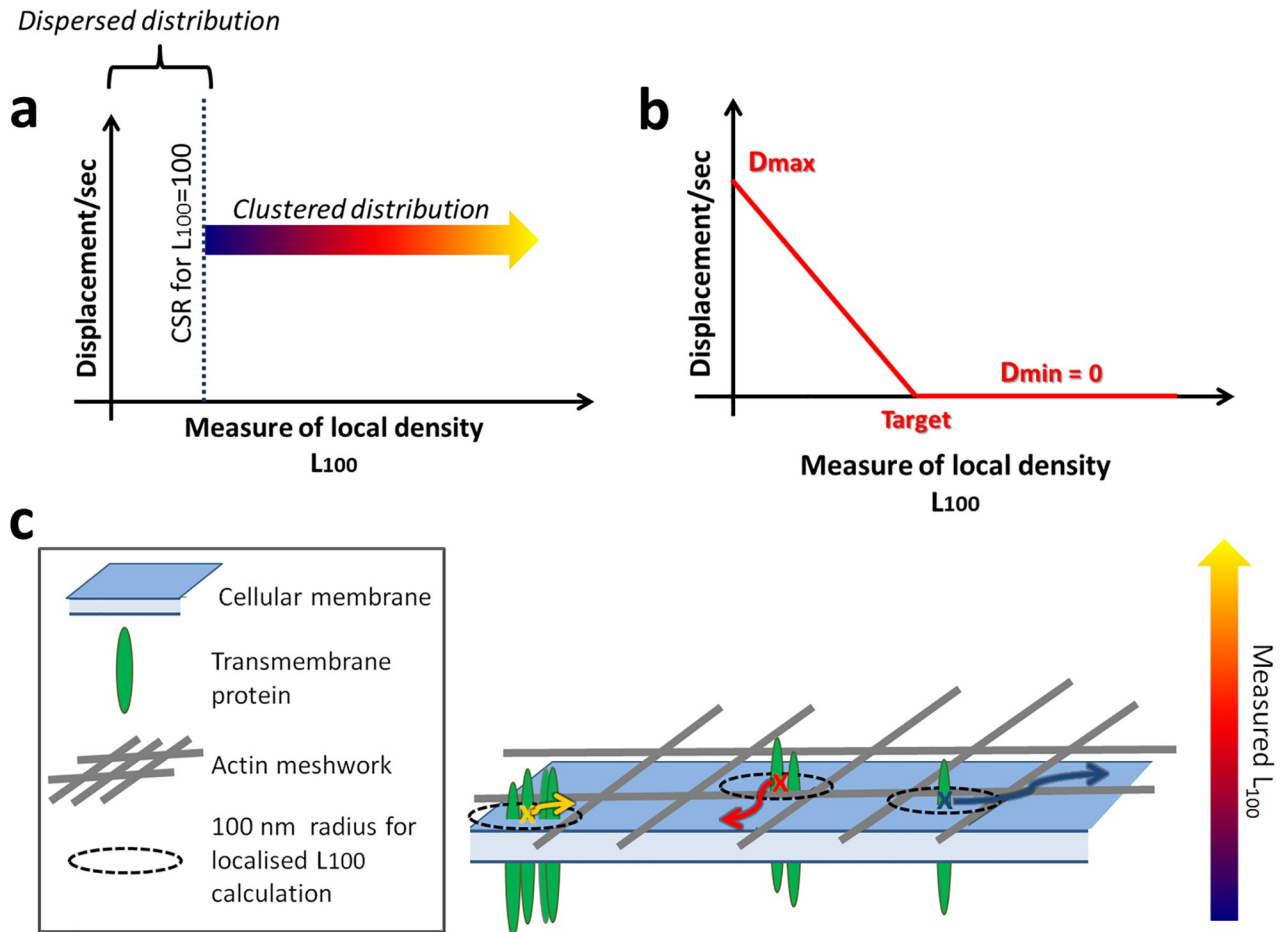
Fig 1. Defining the model. a. Defining the "desire for clustering" as a relation between the L100 value attributed to each molecule and its displacement per second. **b.** Displacement profile applied to each molecule in the Standard Condition. **c.** General model in which the displacement per second of each molecule (colour coded arrows) depends on the local level of clustering (i.e. the number of molecules encircled).

case) up to 69 encircled molecules ($L_{100} \sim 317$) with 2 molecule increments (Fig 2a). The range of targeted L_{100} values recapitulates clustering observed at the cellular membrane using single-molecule localisation, microscopy and quantitative cluster analysis techniques.

Fig 2b consists of representative examples of final frames (after 5 mins simulation) for 5 different target values (7, 25, 45, 55, 67 encircled molecules). They illustrate the agent-molecules reach a clustered distribution within 5 minutes simulations in most cases. These results demonstrate that the use of the "desire for clustering" as a summary of competing cellular processes is sufficient to induce molecular nanoscale aggregation, in turn supporting our initial hypothesis.

The $< \widehat{L}_{100} >$ versus time plots, averaged over n = 30 simulations per condition (Fig 2c), confirm that different outcomes or "regimes" are indeed accessible, depending on the L_{100} target value applied. We can extract two instructive parameters from these curves: the convergence time (Fig 2d) and the associated error (Fig 2e). The convergence time is defined as the amount of time it takes for $< \widehat{L}_{100} >$ to reach a horizontal asymptote that is not equal to the initial CSR value. The error is calculated as: $\frac{<\widehat{L}_{100}> - L_{100,target}}{L_{100,target}}$. Both the convergence time and error highlight that 3 regimes are accessible within our timescale (Fig 2d and 2e). Firstly, the
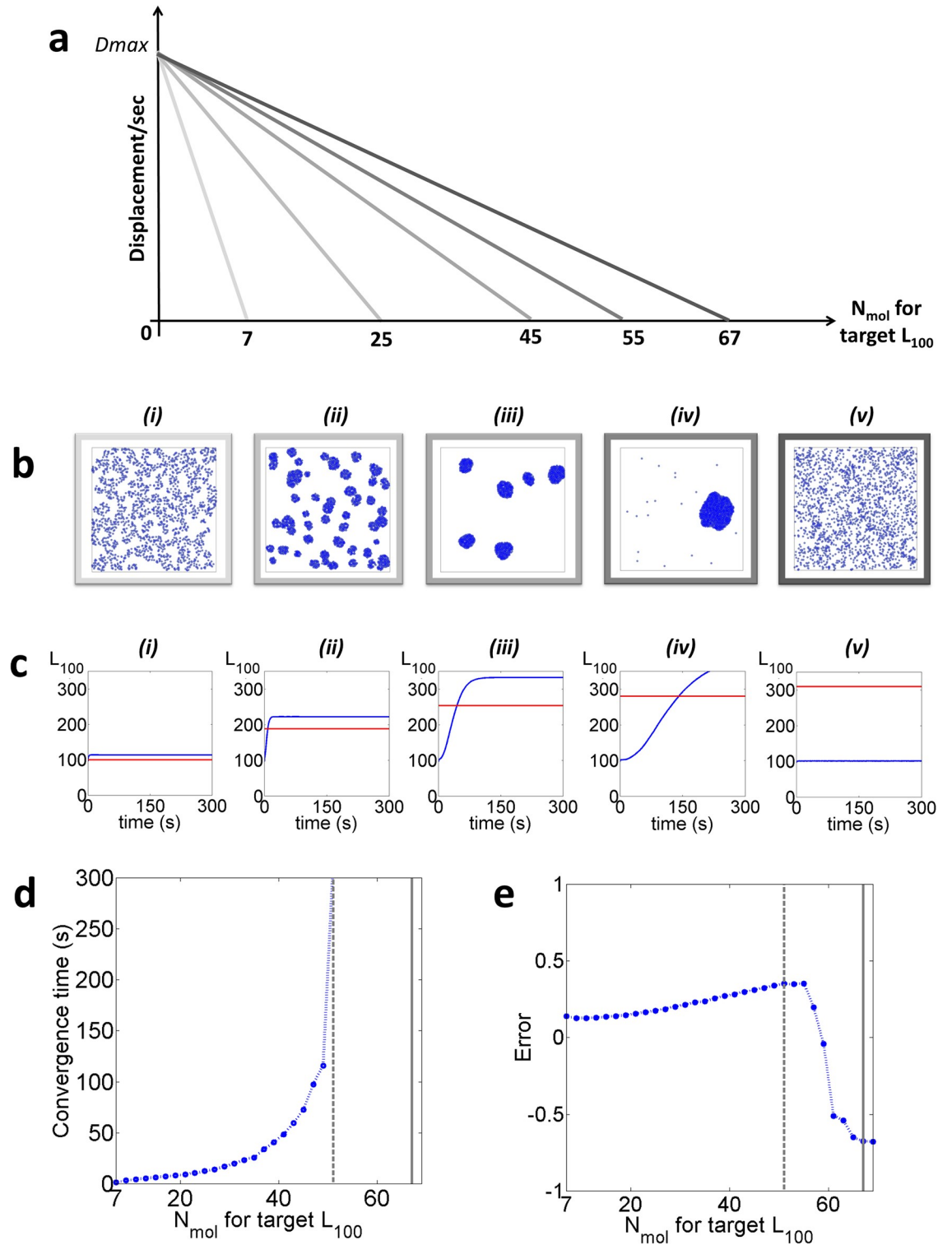
Fig 2. The Standard Condition (n = 30 simulations per condition). a. Examples of displacement profiles applied to the agent-molecules. **b**. Examples of the molecular distributions obtained after 5 min simulations with the target values set at (i) 7, (ii) 25, (iii) 45, (iv) 55, (v) 67 encircled molecules. **c**. Corresponding $< \widehat{L}_{100} >$ values extracted from all molecules over time (depicted blue) and their associated fixed targets (depicted red). **d**. Convergence time and **e.** Error as a function of the number of molecules for each L_{100} target (depicted in blue are the values obtained for each target, in dashed grey the point after which the system takes longer than 5 min to converge and in solid grey, the "cut-off" point).

case of full convergence: $< \widehat{L}_{100} >$ has reached a horizontal asymptote within the 5 minutes timescale (Fig 2b(i)-(iii) and 2c(i)-(iii)). In this case the convergence time varies considerably from one target value to the next, increasing up to 49 encircled molecules, after which no asymptote is reached. The higher the target value is set, the longer the system takes to converge. In terms of error, this regime is associated with a systematic overshooting of the measured $< \widehat{L}_{100} >$ values compared to the target L_{100} value.

The second accessible regime (Fig 2b(iv) and 2c(iv)) similarly consists of a converging system, but for which although displaying an increasing $< \widehat{L}_{100} >$ the horizontal asymptote has not been reached within the allocated 5 minutes timescale (between 51 and 65 encircled molecules).

The last accessible regime however differs drastically from previous cases. It consists of a non-converging system in which the agent-molecules continue to form a CSR distribution over 5 minutes whilst diffusing freely. Interestingly, the switch from converging regimes to CSR is a discontinuous digitized process with a cut-off point existing in the target L_{100} value, after which the agent-molecule does not aggregate further (≥ 67 encircled molecules). We verified that this cut-off point was not in fact a slow convergence by repeating the simulations (target value = 69 encircled molecules) over a total 30 minutes, which demonstrates no sign of convergence (S1 Fig).

Fig 3 summarizes the associated cluster descriptors extracted from the last simulated frame, averaged over the n = 30 simulations for every target L_{100} value condition. These results confirm the existence of 3 possible molecular distribution outcomes, which, in this case translates to: a fully clustered distribution, a clustered distribution with a small ratio of remaining unclustered molecules and finally, a CSR distribution after 5 minutes (Fig 3a). Overall, these results confirm that in most cases the "desire for clustering" is a sufficient rule to induce agent-molecule aggregation. In practice, for the clustered cases the final distribution arises from the appearance of molecular "nucleation sites" in a matter of seconds (S1 Movie). As in cells, an existing cluster appears to facilitate the aggregation of close by molecules[33, 48].

Importantly, our results highlight that for subtle variations of the target value, the resulting molecular distribution present diverse clusters characteristics (Fig 3b–3e). We can generate, for instance, simulations with an average of 5.5 clusters of 95 nm radius with a target set at 45 encircled molecules, whilst a target set at 49 leads to only 3.6 clusters of 114 nm radius. As such, our agent-based model compliments phenomena observed in cells, for which very small changes, for example the engagement of a receptor protein on the PM or the modification of membrane tension are associated with rapid and dramatic changes in molecular clustering. Overall, the clustered distributions obtained via simulation resemble clusters found in cells (their radii varying from 24.5 to 160.2 nm, for instance). These results again verify our initial hypothesis, and more broadly, the validity of the agent-based model presented here for the study molecular aggregation in the PM. As it was the case for the study of the $< \widehat{L}_{100} >$ time-series curves (Fig 2c), detailed cluster descriptors also display a digitized profile with a cut-off point after which the molecules remain in a CSR distribution. This data therefore suggests that clustering itself could be a digitized process with as precise band pass. We further investigated the role of R on the outcome, studying the impact of smaller radius (R = 50nm in S2 Fig) and radius above the diffraction limit (R = 200nm in S3 Fig). In all cases, the three available regimes previously observed (converged, converging, unconverging) are robust to variation in R. Interestingly, the cut-off point appears to be function of R.
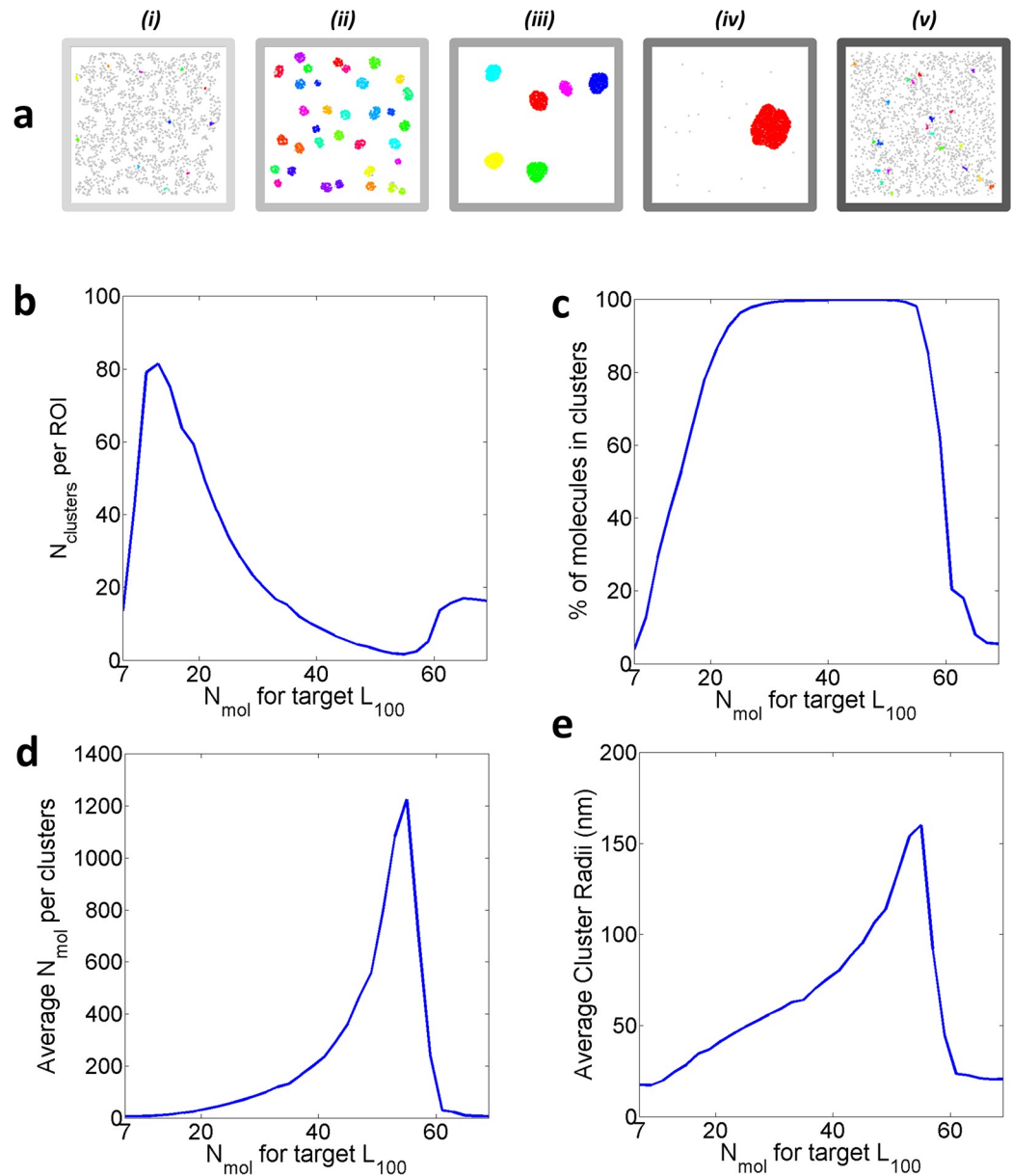
Fig 3. Standard Condition clustering characteristics. a. Example of analysed cluster maps pseudo coloured by cluster identification numbers generated from the final simulated frames with the target set to (i) 7, (ii) 25, (iii) 45, (iv) 55, (v) 67 encircled molecules. For the n = 30 simulations: **b**. Average number of clusters per ROI, **c**. % of clustered molecules, **d**. Average number of molecules per clusters, **e**. Average cluster radius (nm).

Modifying the pre-set rules applied to the agent-molecules

We further study the impact of the pre-set rules applied to the agent-molecules on the measured clustering outcomes. For that purpose, we first varied the parameter D_{max} between a fast and slow diffusion (respectively corresponding to DC~1 $\mu m^2.s^{-1}$ and 0.01 $\mu m^2.s^{-1}$) (Fig 4a). Interestingly, the digitized behaviour, as well as the overall trends of both the $< \widehat{L}_{100} >$ curves and the cluster descriptors initially observed in the Standard Condition, are maintained for both the fast and slow condition. The cut-off value for convergence however appears to be highly dependent on the D_{max} value used for the displacement curves (target value = 59 and 69
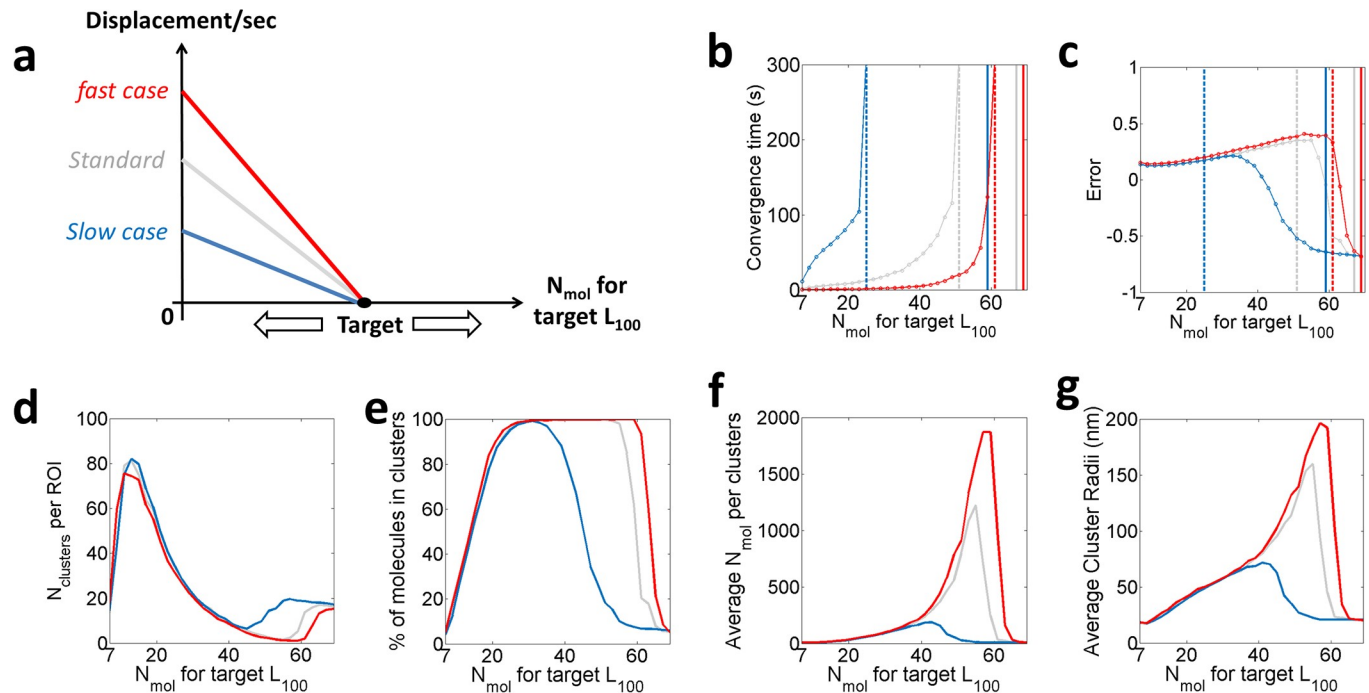
Fig 4. Varying Dmax for n = 30 simulations per condition. In red the fast case (~ 1 μm.s^{-1}), in grey the Standard Condition (~ 0.1 μm.s^{-1}) and in dark blue the slow case (~ 0.01 μm.s^{-1}). **a.** Illustration of the speed profiles applied to the agent-molecules. **b.** Convergence time for the 3 cases, the target after which the system takes longer than 5 minutes to converge (dashed vertical line), and the "cut-off" point (solid vertical line). **c.** Error for each of the 3 D_{max} conditions. **d.** The average number of clusters per ROI. **e.** The % of clustered molecules. **f.** The average number of molecules per clusters. **g.** The average cluster radius (nm), extracted from the final molecular distribution.

https://doi.org/10.1371/journal.pone.0226825.g004

encircled molecules for the fast and slow case respectively) ([Fig 4b and 4c](#)), with slower diffusion leading to a thinner pass band for which the system converges to a clustered distribution.

In particular, these results suggest that faster diffusing molecules tend to aggregate more quickly (i.e. lower convergence time) and over a larger range of target values. As they travel larger distances, fast moving molecules are more likely to be caught within the range of influence of a spontaneous nucleation site (S2 and S3 Movies). For fast diffusing molecules, the associated simulations converge to clustered distributions even for L_{100} targets which do not converge for slower diffusing molecules, whilst forming larger aggregates ([Fig 4d–4g](#)). For instance, for a target set at 63 encircled molecules, the fast diffusing model achieves an average of 7.6 clusters containing an average of 157 molecules while this target remains unclustered for the slow case. Again, our model recapitulates phenomena observed in cells for which faster diffusing molecules result in clustered distribution differing from slowly diffusing molecules. Decreased membrane viscosity, associated with faster diffusing transmembrane proteins, for instance, has been shown to result in more clustered distribution[49].

So far, we have chosen to vary the displacement (or per frame step size) for each molecule over time, which is a robust approximation of Brownian motion at the length scale at which we are studying cluster emergence versus frame update. However, a more general approximation consists in a random walk in which the per-frame step sizes are drawn randomly (and independently) from a normal distribution centred on the targeted diffusion coefficient. Using this approach, we were able to show that not only molecular aggregation can be achieved but also that similar mode (converged, converging, unconverging) are observable (S4 Fig).

We also studied the impact of the shape of displacement curves themselves on the output structures (S5 Fig). Surprisingly, in both non converging-cases, the three possible outcome

regimes (converged, converging, unconverging) remain, with similar values obtained for the cut-off points. This suggests that the digitisation of molecular aggregation is a phenomenon independent of the displacement-clustering relation rule imposed on the agent-molecules. However, the nanoscale structures obtained in both cases differ drastically from the Standard Condition. We further demonstrate that both pores and mobile clusters are achievable within our agent-based model (S4 and S5 Movies). Importantly, both molecular pores[50] and dynamic clusters[51, 52] exist in cellular membranes, highlighting the applicability of our approach to a vast range of molecular nanoscale structures and processes.

We further investigated the impact of D_{min} for non-converging cases. We set D_{min} as the expected per frame displacement of a cluster containing all molecules in the ROI (S6 Fig), 20% of the molecules (S7 Fig) and 10% of the molecules (S8 Fig). In all cases, although, we observe a conservation of the three possible outcomes, the cut-off point itself appears to be highly dependent on D_{min}.

Finally, whilst the use of a linear decay (whether converging or not), is necessary to understand better the mechanism behind the emergence of molecular aggregation, it is unlikely to recapitulate all the variations existing at the cell membrane. We run additional simulations with a desire for clustering following a non-linear decay (quadratic) to verify the robustness of clusters emergence. As in the linear case, we observe molecular aggregation (S9 Fig).

The impact of the actin mesh on molecular aggregation

One of the advantages of performing simulations such as the agent-based model presented here, is that it enables studying the impact of any modifications in the environment architecture on the agents: e.g. would agent behaviour be different in the presence of obstacles or boundaries within the ROI. This approach is particularly interesting in the case of the cellular membrane whose nanoscale architecture is well characterised. Our framework can therefore be used to understand the impact of known cellular structures on the basal level molecular aggregation determined only by the desire for clustering. Here, we focus on the role played by the actin meshwork situated directly beneath the PM. In particular, we compare our Standard Condition with an actin enriched environment. Certainly, as previously stated, the desire for clustering encompasses complex, intertwined and diverse cellular processes, including the potential role of the actin mesh. However, here we are able to study the effect of an increase in filamentous actin added to the desire for clustering as defined in our Standard Condition or basal level of clustering. The environment here remains static, with actin mesh added during the whole time course.

Actin is a fibrous polymer protein which forms a key component of the cell skeleton. It allows the cell to generate forces through actin polymerisation which serves as a highway for molecular trafficking by motor proteins and enhances the cells' structural stability[53–56]. This final function is achieved by a dense meshwork of actin placed immediately below the PM (the actin cortex). Recently, research has focussed on how this cortical actin affects the diffusion and clustering of membrane proteins by essentially forming semi-permeable barriers proximal to the bilayer, transiently confining membrane proteins[57–59]. By modifying the density of this filamentous actin mesh, the enclosed areas of the PM in which molecules can diffuse freely varies. The fact that key signalling pathways from or to the PM are associated with substantial remodelling of the actin meshwork[60–62] tend to sustain these theories of the importance of the actin mesh in regulating molecular aggregation at the PM across multifarious cell types.

In practice, actin fibres are translated into our agent-based model as reflective boundaries arranged in a regular grid, within the ROI. We vary the meshwork density from relatively

sparse (1000 nm spacing) to more dense cases (500 nm and 250 nm spacing). 7 conditions were simulated with: 7, 15, 25, 35, 45, 55 and 65 encircled molecules targets. Representative examples of the molecular distributions obtained after 5 mins simulations are illustrated in Fig 5a–5c. These results suggest that the system can still reach a clustered distribution despite the presence of the additional imposed actin meshwork. These results further highlight that the presence of added actin meshwork and more specifically its density, can modify both the clustering characteristics of the agents and the cut-off point.

We studied the impact of filamentous actin on the overall $< \widehat{L}_{100} >$ trends, similarly to observations made when varying the displacement profile starting point D_{max}. Our simulations reach the cut-off point for a target value smaller than 55, 65 and 65 encircled molecules for 250 nm, 500 nm and 1000 nm mesh spacing respectively. In all cases, the cut-off values consist of smaller values than in the absence of a mesh (i.e. in the Standard Condition). However, although the digitized behaviour is preserved, with varying pass band width depending on the mesh density, our results also suggest that the actin mesh alone, in particular its density, impacts on the characteristics of the molecular aggregates for the same fixed target value. The presence of a dense actin mesh results in agent-molecules reaching a clustered distribution over a very limited range target values, whilst systematically forming more numerous smaller clusters when converging (Fig 5e–5g). For instance, the target value set at 25 encircled molecules in the Standard Condition results in an average of 34 clusters of 57 molecules, whereas in the case of an actin fibres enriched environment, we find an increase in the number of clusters (45.2, 35.7, 34.0 for 250, 500 and 1000nm spacing respectively) containing less molecules (38.1, 53.7, 56.5 for 250, 500 and 1000nm spacing respectively). Additionally, the emergence of large scale aggregation or "protein islands" is also hindered by the presence of these physical barriers. Again, our results compliment phenomena expected with the picket fence model[34] in cells in which actin polymerisation and organisation in regions of dense meshwork is associated with more numerous but importantly, less dense clusters.

Discussion

The cellular membrane has been shown to be a system with a high level of complexity: various processes are known to be involved in the regulation of molecular distributions at the PM. For the most part, these processes (e.g. the picket fence theory, protein affinity, the size exclusion model, membrane thickness, the lipid raft hypothesis) are thought to act locally with often intertwined and competing effects on molecular aggregation. Their complex relationships remain to be fully characterised and more processes are likely to be identified with technological advancement in microscopy. In fact, there is no clear consensus in the field on the role of each in regards of the other[63], as well as strong controversies on the existence of some of these main players (i.e. lipid rafts)[47, 64].

Because of these complex factors, complete and general molecular models, for example atomistic MD simulations of the whole plasma membrane-cortex system, have proven impossible to realise. We suggest in this work that cellular biology will benefit vastly from conceptual models such as agent-based approach as a way to improve our understanding of key cellular processes (e.g. protein clustering at the PM) similarly to other fields with high level of complexity like economics[25]. The agent-based model presented here may lead to simpler ways to study, simulate and interpret molecular clustering in the membrane without using complex biophysical models. We demonstrate that simple local rules obeyed by the agents, can lead to the emergence of aggregation at macroscale. More precisely, we show that the processes acting on molecules in cellular membranes can be summarized in a unique parameter: the "desire for clustering" and that through this framework, the molecular clustering observed in cells can be
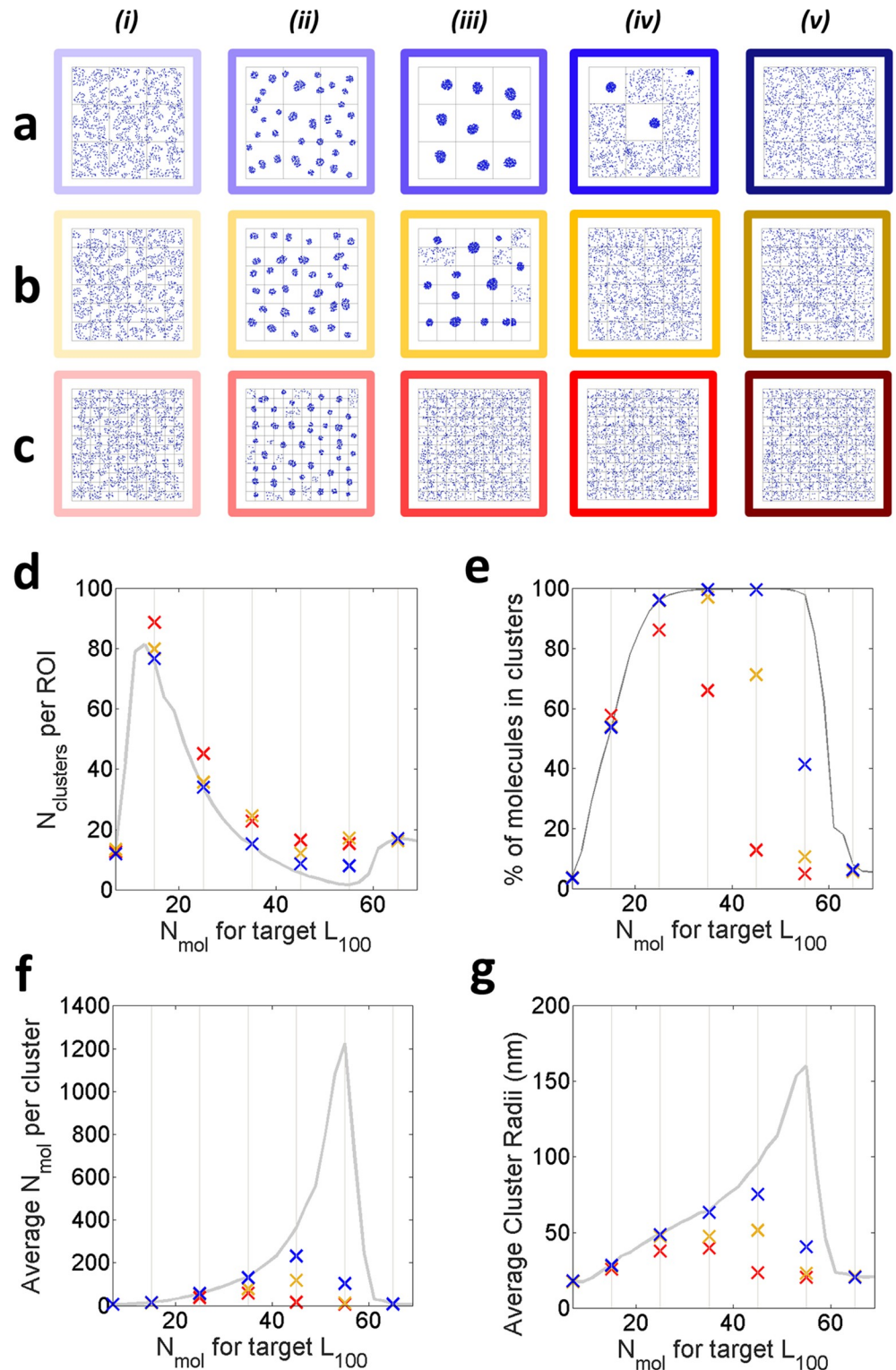
Fig 5. An actin enriched environment. a,b,c. Examples of the molecular distributions obtained after 5 mins simulations with the target encircled molecules set to (i) 7, (ii) 25, (iii) 45, (iv) 55, (v) 65 with 1000 nm, 500 nm and 250 nm spaced actin boundaries respectively. **d**. Average number of clusters per ROI, **e**. % of clustered molecules, **f**. Average number of molecules per clusters, **g**. Average cluster radius (nm). For the n = 30 simulations, the 1000 nm, the 500 nm, 250nm cases are depicted blue, orange and red respectively (the grey curves represent the Standard Condition).

recapitulated. Our results also suggest that clustering itself is a digitized process in addition to clusters ability to digitise the flow of information along signalling pathways.

Interestingly, our simulations highlight that for small variations of the "desire for clustering" applied to molecules, drastically different clustering outcomes are obtained. This mimics observations made in cells where small changes at the PM are associated with significant modifications of the molecular distributions, possibly facilitating signalling or effector functions [65]. Our results also confirm that other known impact of cellular processes on clustering can be recapitulated by the agent-based model presented here. For instance, we show that faster diffusing molecules tend to form more clustered distributions, while enrichment in filamentous actin compared to the basal level, impacts directly on the clusters descriptors with smaller yet more numerous clusters. Both phenomena have been previously observed in cells, demonstrating that the model can generate distributions consistent with those previously observed experimentally. Adding more complex environments, such as non-fully reflective mesh, in which the distribution of agents can evolve, could help further characterise the dependency of cluster emergence to these precise architectures. Dynamic environments, which would allow for temporal variations, could also enable the investigation of the impact of observed cellular processes (such as actin mesh disruption) on protein aggregation.

Agent based models have particular advantages over other methods e.g. MD simulations, which make them particularly useful for applications studying membrane protein distributions and dynamics. Firstly, they do not require complete knowledge of the structure of the system under investigation. They are well suited to the study of emergent phenomena—where macroscale architecture is generated from underlying local forces and they provide a simple and intuitive conceptual framework for understanding how biophysical phenomena (e.g. actin) impact molecular behaviour. In that context, agent based models might be useful for the design of pharmacological interventions designed to alter molecular nanoscale organisation due to their ability to predict the macroscale outcome of a local perturbation. For example, new therapeutic concepts involve the modification of plasma membrane clustering in the context of disease[66].

Supporting information

S1 Fig. 30 min simulation with the target value set at 69 encircled molecules in the Standard Condition, n = 30. a Molecular distribution from t = 0 min to t = 30 min. **b.** Resulting $< \widehat{L}_{100} >$ curve.
(TIF)

S2 Fig. Converging scenario with R = 50nm, (n = 30 simulations per condition). a. Examples of the molecular distributions obtained after 5 min simulations with the target values set at (i) 7, (ii) 25, (iii) 45, (iv) 55, (v) 65 encircled molecules. **b**. Corresponding $< \widehat{L}_{100} >$ values extracted from all molecules over time (depicted blue) and their associated fixed targets (depicted red). **c**. Convergence time and **d**. Error as a function of the number of molecules for each L_{100} target (depicted in blue are the values obtained for each target).
(TIF)

S3 Fig. Converging scenario with R = 200nm, (n = 30 simulations per condition). a. Examples of the molecular distributions obtained after 5 min simulations with the target values set at (i) 7, (ii) 25, (iii) 45, (iv) 55, (v) 65, (vi) 80, (vii) 90 encircled molecules. **b**. Corresponding $< \widehat{L}_{100} >$ values extracted from all molecules over time (depicted blue) and their associated fixed targets (depicted red). **c**. Convergence time and **d**. Error as a function of the number of

molecules for each L_{100} target (depicted in blue are the values obtained for each target).
(TIF)

S4 Fig. Diffusion coefficient extracted from normal distributions, (n = 30 simulations per condition). a. Examples of the molecular distributions obtained after 5 min simulations with the target values set at (i) 7, (ii) 25, (iii) 45, (iv) 55, (v) 65 encircled molecules. **b**. Corresponding $< \widehat{L}_{100} >$ values extracted from all molecules over time (depicted blue) and their associated fixed targets (depicted red). **c**. Convergence time and **d**. Error as a function of the number of molecules for each L_{100} target (depicted in blue are the values obtained for each target).
(TIF)

S5 Fig. Varying the displacement profile. a. Non-converging scenario where a molecule i is immobile for L100,i = L100,target only. **b.** Converging scenario with $D_{min} > 0$. **c.** Example of final updates frame for target set at 7, 25, 45, 65 encircled molecules, in the non-converging scenario. **d.** Example of final updates frame for target set at 7, 25, 45, 65 encircled molecules in the converging scenario with $D_{min} > 0$.
(TIF)

S6 Fig. Converging scenario with $D_{min} \sim 0.52$ nm.ms^{-1}, (n = 10 simulations per condition). **a**. Examples of the molecular distributions obtained after 5 min simulations with the target values set at (i) 7, (ii) 25, (iii) 45, (iv) 55, (v) 65, encircled molecules. **b**. Corresponding $< \widehat{L}_{100} >$ values extracted from all molecules over time (depicted blue) and their associated fixed targets (depicted red). **c**. Convergence time and **d**. Error as a function of the number of molecules for each L_{100} target (depicted in blue are the values obtained for each target).
(TIF)

S7 Fig. Converging scenario with $D_{min} \sim 0.78$ nm.ms^{-1}, (n = 10 simulations per condition). **a**. Examples of the molecular distributions obtained after 5 min simulations with the target values set at (i) 7, (ii) 25, (iii) 45, (iv) 55, (v) 65 encircled molecules. **b**. Corresponding $< \widehat{L}_{100} >$ values extracted from all molecules over time (depicted blue) and their associated fixed targets (depicted red). **c**. Convergence time and **d**. Error as a function of the number of molecules for each L_{100} target (depicted in blue are the values obtained for each target).
(TIF)

S8 Fig. Converging scenario with $D_{min} \sim 0.93$ nm.ms^{-1}, (n = 10 simulations per condition). **a**. Examples of the molecular distributions obtained after 5 min simulations with the target values set at (i) 7, (ii) 25, (iii) 45, (iv) 55, (v) 65 encircled molecules. **b**. Corresponding $< \widehat{L}_{100} >$ values extracted from all molecules over time (depicted blue) and their associated fixed targets (depicted red). **c**. Convergence time and **d**. Error as a function of the number of molecules for each L_{100} target (depicted in blue are the values obtained for each target).
(TIF)

S9 Fig. Quadratic decay, (n = 30 simulations per condition). a. decay used for the displacement calculation of each molecule at each frame. **b**. Example of the molecular distributions obtained after 5 min. **c**. Corresponding $< \widehat{L}_{100} >$ values extracted from all molecules over time (depicted blue).
(TIF)

S1 Movie. Diffusing molecules over the 5 minutes simulation with 1 frame per sec, sped 10 times, in the Standard Condition. Target value: 41 encircled molecules.
(AVI)

S2 Movie. Diffusing molecules over the 5 minutes simulation with 1 frame per sec, sped 10 times, in the case of slowly diffusing molecules. Target value: 41 encircled molecules. (AVI)

S3 Movie. Diffusing molecules over the 5 minutes simulation with 1 frame per sec, sped 10 times, in the case of fast diffusing molecules. Target value: 41 encircled molecules. (AVI)

S4 Movie. Diffusing molecules over the 5 minutes simulation with 1 frame per sec, sped 10 times, with a non-converging displacement profile applied to agent-molecules. Target value: 41 encircled molecules. (AVI)

S5 Movie. Diffusing molecules over the 5 minutes simulation with 1 frame per sec, sped 10 times, with a converging displacement profile for which $D_{min} > 0$ applied to agent-molecules. Target value: 35 encircled molecules. (AVI)

Author Contributions

Conceptualization: Juliette Griffié, Dylan M. Owen.

Investigation: Juliette Griffié.

Methodology: Juliette Griffié, Ruby Peters.

Software: Juliette Griffié.

Supervision: Dylan M. Owen.

Validation: Juliette Griffié.

Writing – original draft: Juliette Griffié, Dylan M. Owen.

Writing – review & editing: Juliette Griffié, Ruby Peters, Dylan M. Owen.

References

1. Singer SJ, Nicolson GL. The fluid mosaic model of the structure of cell membranes. Science. 1972; 175:720–31. https://doi.org/10.1126/science.175.4023.720 PMID: 4333397

2. Groves JT, Kuriyan J. Molecular mechanisms in signal transduction at the membrane. Nature Structural and Molecular Biology. 2010; 17(6):659–65. https://doi.org/10.1038/nsmb.1844 PMID: 20495561

3. Kusumi A, Fujiwara TK, Chadda R, Xie M, Tsunoyama TA, Kalay Z, et al. Dynamic Organizing Principles of the Plasma Membrane that Regulate Signal Transduction: Commemorating the Fortieth Anniversary of Singer and Nicolson's Fluid-Mosaic Model. Annual Review of Cell and Developmental Biology. 2012; 28(1):215–50. https://doi.org/10.1146/annurev-cellbio-100809-151736 PMID: 22905956.

4. Griffié J, Burn G, Owen DM. The nanoscale organization of signaling domains at the plasma membrane. Curr Top Membr. 2015; 75:125–65. https://doi.org/10.1016/bs.ctm.2015.03.004 PMID: 26015282.

5. Cebecauer M, Spitaler M, Serge A, Magee AI. Signalling complexes and clusters: functional advantages and methodological hurdles. Journal of Cell Science. 2010; 123(3):309–20. https://doi.org/10.1242/jcs.061739 PMID: 20130139

6. Willig KI, Rizzoli SO, Westphal V, Jahn R, Hell SW. STED microscopy reveals that synaptotagmin remains clustered after synaptic vesicle exocytosis. Nature. 2006; 440:935. https://doi.org/10.1038/nature04592 https://www.nature.com/articles/nature04592#supplementary-information. PMID: 16612384

7. Mohrmann R, de Wit H, Verhage M, Neher E, Sørensen JB. Fast Vesicle Fusion in Living Cells Requires at Least Three SNARE Complexes. Science. 2010; 330(6003):502. https://doi.org/10.1126/science.1193134 PMID: 20847232

8. Neve-Oz Y, Razvag Y, Sajman J, Sherman E. Mechanisms of localized activation of the T cell antigen receptor inside clusters. Biochimica et Biophysica Acta (BBA)—Molecular Cell Research. 2015; 1853 (4):810–21. http://dx.doi.org/10.1016/j.bbamcr.2014.09.025.

9. Sherman E, Barr V, Manley S, Patterson G, Balagopalan L, Akpan I, et al. Functional Nanoscale Organization of Signaling Molecules Downstream of the T Cell Antigen Receptor. Immunity. 2011; 35 (5):705–20. https://doi.org/10.1016/j.immuni.2011.10.004 PMID: 22055681

10. Dustin ML, Groves JT. Receptor Signaling Clusters in the Immune Synapse. Annual Review of Biophysics. 2012; 41(1):543–56. https://doi.org/10.1146/annurev-biophys-042910-155238 PMID: 22404679

11. Prior IA, Parton RG, Hancock JF. Observing Cell Surface Signaling Domains Using Electron Microscopy. Science STKE. 2003; 2003(177):pl9-.

12. Prior IA, Muncke C, Parton RG, Hancock JF. Direct visualization of Ras proteins in spatially distinct cell surface microdomains. J Cell Biol. 2003; 160(2):165–70. https://doi.org/10.1083/jcb.200209091 PMID: 12527752

13. Prior IA, Harding A, Yan J, Sluimer J, Parton RG, Hancock JF. GTP-dependent segregation of H-ras from lipid rafts is required for biological activity. Nature Cell Biology. 2001; 3(4):368–75. https://doi.org/10.1038/35070050 PMID: 11283610

14. Rust MJ, Bates M, Zhuang X. Sub-diffraction-limit imaging by stochastic optical reconstruction microscopy (STORM). Nature Methods. 2006; 3(10):793–6. https://doi.org/10.1038/nmeth929 PMID: 16896339

15. Klar TA, Jakobs S, Dyba M, Egner A, Hell SW. Fluorescence microscopy with diffraction resolution barrier broken by stimulated emission. Proceedings of the National Academy of Sciences. 2000; 97 (15):8206–10.

16. Betzig E, Patterson GH, Sougrat R, Lindwasser OW, Olenych S, Bonifacino JS, et al. Imaging Intracellular Fluorescent Proteins at Nanometer Resolution. Science. 2006; 313:1642–5. https://doi.org/10.1126/science.1127344 PMID: 16902090

17. Roob E III, Trendel N, Rein ten Wolde P, Mugler A. Cooperative Clustering Digitizes Biochemical Signaling and Enhances its Fidelity. Biophysical Journal. 2016; 110(7):1661–9. https://doi.org/10.1016/j.bpj.2016.02.031 PMID: 27074690

18. Kenworthy AK. Nanoclusters digitize Ras signalling. Nature Cell Biology. 2007; 9(8):875–7. https://doi.org/10.1038/ncb0807-875 PMID: 17671455

19. Lewitzky M, Simister PC, Feller SM. Beyond 'furballs' and 'dumpling soups'–towards a molecular architecture of signaling complexes and networks. FEBS Letters. 2012; 586(17):2740–50. https://doi.org/10.1016/j.febslet.2012.04.029 PMID: 22710161

20. Dharan N, Farago O. Interplay between membrane elasticity and active cytoskeleton forces regulates the aggregation dynamics of the immunological synapse. Soft Matter. 2017; 13(38):6938–46. https://doi.org/10.1039/c7sm01064h PMID: 28825081

21. Epstein JM. Agent-based computational models and generative social science. Complexity. 1999; 4(5):41–60. https://doi.org/10.1002/(SICI)1099-0526(199905/06)4:5<41::AID-CPLX9>3.0.CO;2-F

22. Berry BJL, Kiel LD, Elliott E. Adaptive agents, intelligence, and emergent human organization: Capturing complexity through agent-based modeling. Proceedings of the National Academy of Sciences. 2002; 99(suppl 3):7187–8. https://doi.org/10.1073/pnas.092078899 PMID: 11997449

23. Tesfatsion L. Agent-based computational economics: modeling economies as complex adaptive systems. Information Sciences. 2003; 149(4):262–8. https://doi.org/10.1016/S0020-0255(02)00280-3.

24. Richiardi MG. Agent-based computational economics: a short introduction. The Knowledge Engineering Review. 2012; 27(2):137–49. Epub 04/26. https://doi.org/10.1017/S0269888912000100

25. Farmer JD, Foley D. The economy needs agent-based modelling. Nature. 2009; 460:685. https://doi.org/10.1038/460685a PMID: 19661896

26. Lingwood D, Simons K. Lipid Rafts As a Membrane-Organizing Principle. Science. 2010; 327 (5961):46–50. https://doi.org/10.1126/science.1174621 PMID: 20044567

27. Pizzo P, Viola A. Lipid rafts in lymphocyte activation. Microbes and Infection. 2004; 6(7):686–92. https://doi.org/10.1016/j.micinf.2004.02.017 PMID: 15158776

28. van Meer G. Invisible rafts at work. Traffic. 2004; 5(4):211–2. https://doi.org/10.1111/j.1600-0854.2004.00176.x PMID: 15030562

29. Pike LJ. Lipid rafts: bringing order to chaos. Journal of Lipid Research. 2003; 44(4):655–67. https://doi.org/10.1194/jlr.R200021-JLR200 PMID: 12562849

30. Edidin M. The state of lipid rafts: From model membranes to cells. Annual Review of Biophysics and Biomolecular Structure. 2003; 32(1):257–83.

31. Magee T, Pirinen N, Adler J, Pagakis SN, Parmryd I. Lipid rafts: cell surface platforms for T cell signaling. Biological Research. 2002; 35(2):127–31. https://doi.org/10.4067/s0716-97602002000200003 PMID: 12415729

32. Simons K, Ikonen E. Functional rafts in cell membranes. Nature. 1997; 387:569–72. https://doi.org/10.1038/42408 PMID: 9177342

33. Schmid EM, Bakalar MH, Choudhuri K, Weichsel J, Ann HS, Geissler PL, et al. Size-dependent protein segregation at membrane interfaces. Nature Physics. 2016;advance online publication. https://doi.org/10.1038/nphys3678 http://www.nature.com/nphys/journal/vaop/ncurrent/abs/nphys3678.html#supplementary-information. PMID: 27980602

34. Kusumi A, Sako Y. Cell surface organization by the membrane skeleton. Current Opinion in Cell Biology. 1996; 8(4):566–74. https://doi.org/10.1016/S0955-0674(96)80036-6https://doi.org/10.1016/s0955-0674(96)80036-6 PMID: 8791449

35. Sengupta P, Jovanovic-Talisman T, Skoko D, Renz M, Veatch SL, Lippincott-Schwartz J. Probing protein heterogeneity in the plasma membrane using PALM and pair correlation analysis. Nature Methods. 2011; 8(11):969–75. http://www.nature.com/nmeth/journal/v8/n11/abs/nmeth.1704.html#supplementary-information. https://doi.org/10.1038/nmeth.1704 PMID: 21926998

36. Jayasinghe I, Clowsley AH, Lin R, Lutz T, Harrison C, Green E, et al. True Molecular Scale Visualization of Variable Clustering Properties of Ryanodine Receptors. Cell Reports. 2018; 22(2):557–67. https://doi.org/10.1016/j.celrep.2017.12.045. PMID: 29320748

37. Burn GL, Cornish GH, Potrzebowska K, Samuelsson M, Griffié J, Minoughan S, et al. Superresolution imaging of the cytoplasmic phosphatase PTPN22 links integrin-mediated T cell adhesion with autoimmunity. Science Signaling. 2016; 9(448):ra99. https://doi.org/10.1126/scisignal.aaf2195 PMID: 27703032

38. Griffié J, Shlomovich L, Williamson DJ, Shannon M, Aaron J, Khuon S, et al. 3D Bayesian cluster analysis of super-resolution data reveals LAT recruitment to the T cell synapse. Scientific Reports. 2017; 7 (1):4077. https://doi.org/10.1038/s41598-017-04450-w PMID: 28642595

39. Owen DM, Rentero C, Rossy J, Magenau A, Williamson D, Rodriguez M, et al. PALM imaging and cluster analysis of protein heterogeneity at the cell surface. Journal of Biophotonics. 2010; 3(7):446–54. https://doi.org/10.1002/jbio.200900089 PMID: 20148419

40. Pageon SV, Cordoba S-P, Owen DM, Rothery SM, Oszmiana A, Davis DM. Superresolution Microscopy Reveals Nanometer-Scale Reorganization of Inhibitory Natural Killer Cell Receptors upon Activation of NKG2D. Science Signaling. 2013; 6(285):ra62-. https://doi.org/10.1126/scisignal.2003947 PMID: 23882121

41. Claus J, Patel G, Autore F, Colomba A, Weitsman G, Soliman TN, et al. Inhibitor-induced HER2-HER3 heterodimerisation promotes proliferation through a novel dimer interface. eLife. 2018; 7:e32271. https://doi.org/10.7554/eLife.32271 PMID: 29712619

42. Griffie J, Shannon M, Bromley CL, Boelen L, Burn GL, Williamson DJ, et al. A Bayesian cluster analysis method for single-molecule localization microscopy data. Nature Protocols. 2016; 11(12):2499–514. https://doi.org/10.1038/nprot.2016.149 http://www.nature.com/nprot/journal/v11/n12/abs/nprot.2016.149.html#supplementary-information. PMID: 27854362

43. Rubin-Delanchy P, Burn GL, Griffie J, Williamson DJ, Heard NA, Cope AP, et al. Bayesian cluster identification in single-molecule localization microscopy data. Nature Methods. 2015; 12(11):1072–6. https://doi.org/10.1038/nmeth.3612 http://www.nature.com/nmeth/journal/vaop/ncurrent/abs/nmeth.3612.html#supplementary-information. PMID: 26436479

44. Griffié J, Boelen L, Burn G, Cope AP, Owen DM. Topographic prominence as a method for cluster identification in single-molecule localisation data. Journal of Biophotonics. 2015; 9(11):925–34. https://doi.org/10.1002/jbio.201400127 PMID: 25663080

45. Lommerse PHM, Snaar-Jagalska BE, Spaink HP, Schmidt T. Single-molecule diffusion measurements of H-Ras at the plasma membrane of live cells reveal microdomain localization upon activation. Journal of Cell Science. 2005; 118(9):1799–809. https://doi.org/10.1242/jcs.02300 PMID: 15860728

46. Owen DM, Williamson D, Rentero C, Gaus K. Quantitative microscopy: protein dynamics and membrane organisation. Traffic. 2009; 10(8):962–71. Epub 2009/05/07. https://doi.org/10.1111/j.1600-0854.2009.00908.x PMID: 19416480

47. Honigmann A, Mueller V, Ta H, Schoenle A, Sezgin E, Hell SW, et al. Scanning STED-FCS reveals spatiotemporal heterogeneity of lipid interaction in the plasma membrane of living cells. Nature Communications. 2014; 5. https://doi.org/10.1038/ncomms6412 PMID: 25410140

48. Germain RN. Computational analysis of T cell receptor signaling and ligand discrimination—Past, present, and future. FEBS Letters. 2010; 584(24):4814–22. https://doi.org/10.1016/j.febslet.2010.10.027 PMID: 20965176

49. Owen DM, Williamson DJ, Magenau A, Gaus K. Sub-resolution lipid domains exist in the plasma membrane and regulate protein diffusion and distribution. Nature Communications. 2012; 3:1256. http://www.nature.com/ncomms/journal/v3/n12/suppinfo/ncomms2273_S1.html. https://doi.org/10.1038/ncomms2273 PMID: 23212385

50. Löschberger A, van de Linde S, Dabauvalle M-C, Rieger B, Heilemann M, Krohne G, et al. Super-resolution imaging visualizes the eightfold symmetry of gp210 proteins around the nuclear pore complex and resolves the central channel with nanometer resolution. Journal of Cell Science. 2012; 125(3):570–5. https://doi.org/10.1242/jcs.098822 PMID: 22389396

51. Ketchum C, Miller H, Song W, Upadhyaya A. Ligand Mobility Regulates B Cell Receptor Clustering and Signaling Activation. Biophysical Journal. 2014; 106(1):26–36. https://doi.org/10.1016/j.bpj.2013.10.043 PMID: 24411234

52. Juliette G, BG L, WD J, Ruby P, Patrick RD, OD M. Dynamic Bayesian Cluster Analysis of Live-Cell Single Molecule Localization Microscopy Datasets. Small Methods. 0(0):1800008. https://doi.org/10.1002/smtd.201800008

53. Salbreux G, Charras G, Paluch E. Actin cortex mechanics and cellular morphogenesis. Trends in Cell Biology. 2012; 22(10):536–45. https://doi.org/10.1016/j.tcb.2012.07.001 PMID: 22871642

54. Parsons JT, Horwitz AR, Schwartz MA. Cell adhesion: integrating cytoskeletal dynamics and cellular tension. Nature Reviews Molecular Cell Biology. 2010; 11(9):633–43. http://www.nature.com/nrm/journal/v11/n9/suppinfo/nrm2957_S1.html. https://doi.org/10.1038/nrm2957 PMID: 20729930

55. Beemiller P, Krummel MF. Mediation of T-Cell Activation by Actin Meshworks. Cold Spring Harbor Perspectives in Biology. 2010; 2(9). https://doi.org/10.1101/cshperspect.a002444 PMID: 20702599

56. Krummel MF, Macara I. Maintenance and modulation of T cell polarity. Nature Immunology. 2006; 7(11):1143–9. https://doi.org/10.1038/ni1404 PMID: 17053799

57. Albrecht D, Winterflood CM, Sadeghi M, Tschager T, Noé F, Ewers H. Nanoscopic compartmentalization of membrane protein motion at the axon initial segment. The Journal of Cell Biology. 2016.

58. Xu K, Zhong G, Zhuang X. Actin, Spectrin, and Associated Proteins Form a Periodic Cytoskeletal Structure in Axons. Science. 2013; 339(6118):452–6. https://doi.org/10.1126/science.1232251 PMID: 23239625

59. Dustin ML. Cell adhesion molecules and actin cytoskeleton at immune synapses and kinapses. Current Opinion in Cell Biology. 2007; 19(5):529–33. https://doi.org/10.1016/j.ceb.2007.08.003 PMID: 17923403

60. Gowrishankar K, Ghosh S, Saha S, C R, Mayor S, Rao M. Active Remodeling of Cortical Actin Regulates Spatiotemporal Organization of Cell Surface Molecules. Cell. 2012; 149(6):1353–67. https://doi.org/10.1016/j.cell.2012.05.008 PMID: 22682254

61. Babich A, Li S, O'Connor RS, Milone MC, Freedman BD, Burkhardt JK. F-actin polymerization and retrograde flow drive sustained PLCγ1 signaling during T cell activation. The Journal of Cell Biology. 2012; 197(6):775–87. https://doi.org/10.1083/jcb.201201018 PMID: 22665519

62. Chaudhuri A, Bhattacharya B, Gowrishankar K, Mayor S, Rao M. Spatiotemporal regulation of chemical reactions by active cytoskeletal remodeling. Proceedings of the National Academy of Sciences. 2011; 108(36):14825–30. https://doi.org/10.1073/pnas.1100007108 PMID: 21873247

63. Bernardino de la Serna J, Schütz GJ, Eggeling C, Cebecauer M. There Is No Simple Model of the Plasma Membrane Organization. Frontiers in Cell and Developmental Biology. 2016; 4(106). https://doi.org/10.3389/fcell.2016.00106 PMID: 27747212

64. Munro S. Lipid rafts: Elusive or illusive? Cell. 2003; 115(4):377–88. https://doi.org/10.1016/s0092-8674(03)00882-1 PMID: 14622593

65. Lingwood D, Ries J, Schwille P, Simons K. Plasma membranes are poised for activation of raft phase coalescence at physiological temperature. Proceedings of the National Academy of Sciences. 2008; 105(29):10005–10.

66. Najumudeen AK, Jaiswal A, Lectez B, Oetken-Lindholm C, Guzman C, Siljamaki E, et al. Cancer stem cell drugs target K-ras signaling in a stemness context. Oncogene. 2016; 35(40):5248–62. https://doi.org/10.1038/onc.2016.59 PMID: 26973241